A Three-State Nonadiabatic Model for Intramolecular Electronic Energy Transfer (IEET) in 9-Anthryl-1′-naphthylalkanes Studied by Molecular Mechanics/Valence Bond Dynamics

Franck Jolibois,*,‡,§ Michael J. Bearpark,‡ Stéphane Klein,‡ Massimo Olivucci,*,† and Michael A. Robb*,‡

Contribution from the Department of Chemistry, King's College London, Strand, London WC2R 2LS, United Kingdom, and Istituto di Chimica Organica, Università degli Studi di Siena, Pian dei Mantellini, 44 I-53100 Siena, Italy

Received July 30, 1999. Revised Manuscript Received April 21, 2000

Abstract: Classical trajectory simulations with the inclusion of nonadiabatic transitions have been used to study intramolecular electronic energy transfer (IEET) in 9-anthryl-1′-naphthylalkanes. We provide evidence that a model with two geometric coordinates (the naphthalene transannular bond and the anthracene transannular bonds) and involving three covalent (dot-dot) singlet diabatic states (**N*-A**, **N*-A*** and **N-A***) is needed to describe the mechanistic aspects of IEET in these systems. Although the computations show that the initial photoexcitation is to the third covalent state, which corresponds to the **N*-A** state in the Franck−Condon region, the process of IEET occurs on the lowest energy covalent state. Dynamics results show that intramolecular vibrational redistribution (IVR) on the lowest energy covalent state into the anthracene transannular vibrations on the **N*-A** diabatic potential surface is faster for the naphthalene−$(CH_2)_3$−anthracene system, where interchromphoric exchange interactions are possible due to a "sandwich" type conformation, than for the naphthalene−$(CH_2)_1$−anthracene system where a more rigid "spacer" (one CH_2 group) only allows a "T" shape conformation. A similar conclusion can be drawn for the transition from the **N*-A*** diabatic surface to the **N-A***diabatic surface.

Introduction

Intramolecular electronic energy transfer (IEET) is involved in photosynthesis, light harvesting, polymer photophysics, and photochemical synthesis and thus is of fundamental importance in biology, chemistry, and physics.[1] The IEET process can be studied experimentally when a donor D, in a bichromophoric system D−A, is excited to an excited-state D* and emission is detected from an acceptor A*.

One of the first observations of intramolecular electronic energy transfer in a simple bichromophoric system was documented for a series of 9-anthryl-1′-naphthylalkanes, at room temperature in solution[2] (see Figure 1). More recently, Speiser and co-workers have studied two of these molecules (Figure 1), namely 9-(1-naphthylmethyl)anthracene (**A1N**) and 9-(3-(1-naphthyl)propyl)anthracene (**A3N**), under jet-cooled conditions.[3] In the latter experiments, the specific excitation of the donor naphthalene chromophore (to the donor N*) in **A3N** ($n = 3$ in Figure 1) resulted in anthracene emission (from the acceptor A*) only. In contrast, naphthalene absorption in **A1N** ($n = 1$ in Figure 1) leads to emission from both chromophores with much slower quenching. Thus, the energy transfer process is complete for **A3N** whereas the IEET process is less inefficient for **A1N**. Because of this difference in behavior, these molecules constitute good prototype models for the experimental and theoretical study of electronic energy transfer (IEET).

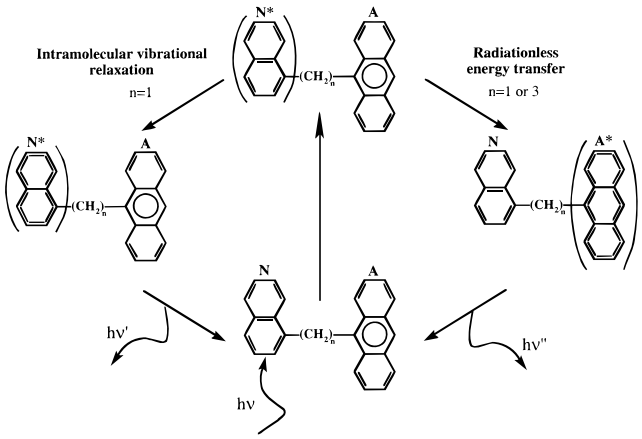

Figure 1. Schematic representation of the energy transfer process in **A1N** ($n = 1$) and **A3N** ($n = 3$). In the left side of the figure emission occurs from the excited **N*** moiety and no IEET has occurred. In the right side of the figure, one has energy transfer to the excited **A*** moiety followed by emission.

The rates of IEET processes are usually interpreted in terms of phenomenological models such as those proposed by Förster[4−6] and Dexter.[7] A good discussion of these methods

* Address correspondence to this author.
‡ King's College London.
‡ Istituto di Chimica Organica.
§ Permanent address: Laboratoire de physique quantique, IRSAMC, Université Paul Sabatier, 118 route de Narbonne, 31062 Toulouse Cedex (France).

(1) Speiser, S. *Chem. Rev.* **1996**, *96*, 1953−1976.
(2) Schnepp, O.; Levy, M. *J. Am. Chem. Soc.* **1962**, *84*, 172−177.
(3) Rosenblum, G.; Grosswasser, D.; Schael, F.; Rubin, M. B.; Speiser, S. *Chem. Phys. Lett.* **1996**, *263*, 441−448.
(4) Förster, Th. *Ann. Phys. (Leipzig)* **1948**, *2*, 5.
(5) Förster, Th. *Discuss Faraday Soc*. **1959**, *27*, 7.
(6) Förster, Th. In *Modern quantum chemistry*; Sinanoglu, O., Ed.; Academic Press: New York, 1968; Vol. 3, p 93.
(7) Dexter, D. L. *J. Chem. Phys.* **1953**, *2*, 836−850.

10.1021/ja992717w CCC: $19.00
Published on Web 06/21/2000

Scheme 1

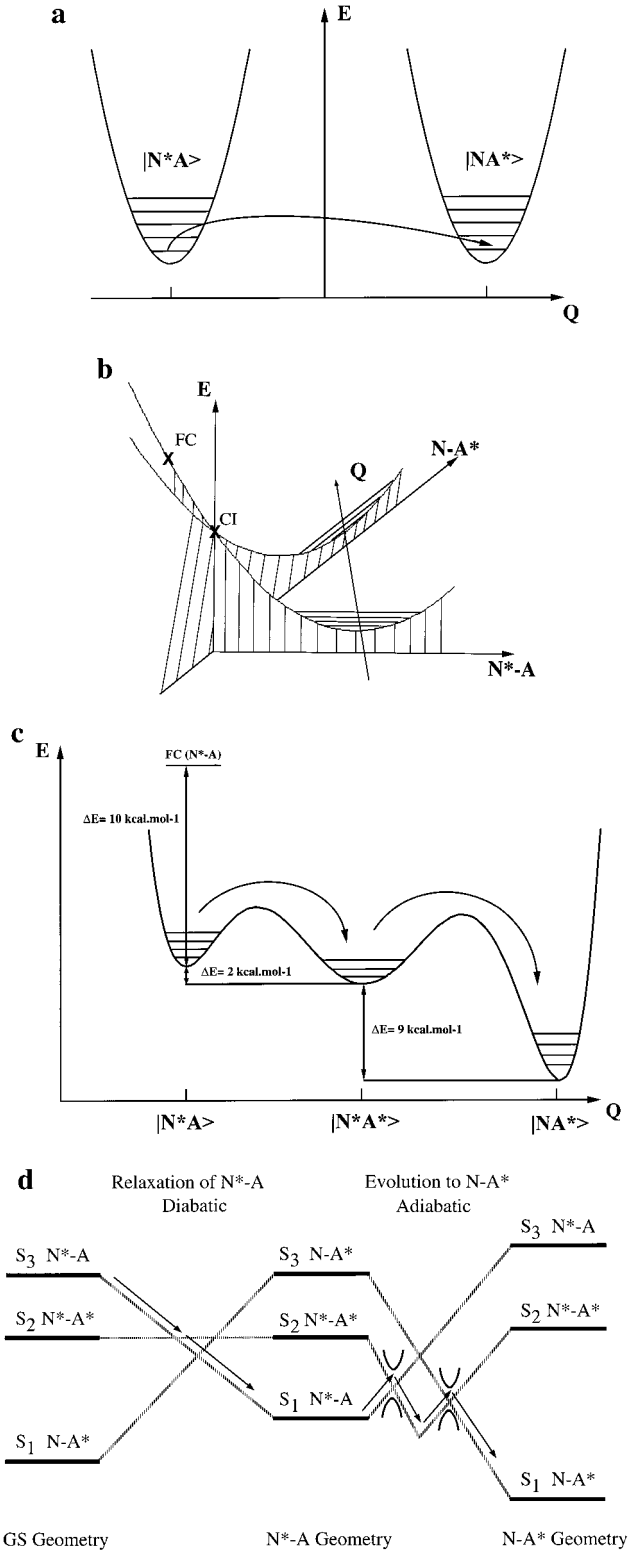

can be found in the review of Speiser.[1] In these theories, the *rate* of the **N*-A → N-A*** process is correlated with the vibrational wave function overlaps, long-range Coulombic forces, and dipole−dipole interactions. The energy transfer process is viewed like an electronic excitation process as illustrated in Scheme 1a. Until recently, most reported studies on IEET were performed in solution where the solvent induces a complete relaxation of the donor and acceptor excited states prior to the transfer event. In a supersonic jet expansion, IEET has to be considered from a specific excited vibronic state of the donor and recent experiments suggest that the IEET process may depend on the particular vibronic excitation.[3,8−10] Thus for vibrationally unrelaxed systems, the general features of IEET might not be consistent with either the simple Fermi Golden Rule type formalism or the Förster/Dexter models.[11]

In this work we shall focus on the *mechanism* of IEET presented as a traditional chemical *reaction path* followed by the nuclei as the reaction progresses over one or more potential energy surfaces (see Scheme 1c). Thus our objective is to show how the electronic excitation can be transferred from one part of the molecular system to another by elucidating the details of nuclear motion along which this occurs (thus we are interested in the nature of Q itself, the reaction path shown in Scheme 1c). Since for IEET the reaction is nonadiabatic, the mechanistic pathway has been mapped out by computing classical trajectories involving three potential surfaces with nonadiabatic dynamics[12−16] using all of the nuclear variables together with a treatment of nonadiabatic effects. In this picture, excitation of the molecule places the system on an excited potential surface where the force field experienced by the nuclei is different from the ground state. Accordingly the nuclei relax (under this excited state force field) to trace out a reaction path (Q in Scheme 1, paths a, b, or c) to the products. The study of the relaxation process in this way gives mechanistic information (a reaction path) but can never yield a rate. Since only a small region of phase space is explored in this way, the information is qualitative but complementary to the usual models used to fit experimental IEET data.

Naphthalene and anthracene have two low-lying electronic excited states: B_{3u} (or L_b), which is long axis (x) polarized, and B_{2u} (or L_a), which is short axis (y) polarized. The L_b state is a covalent state (dot-dot) while the L_a state is zwitterionic (+ − hole-pair). For naphthalene the L_b state is lower than the L_a state, while for anthracene, the L_a lies lowest in energy. In the case of naphthalene, the pure electronic transition to the L_b state has very low intensity because the transition is from the ground covalent state to a covalent excited state. In fact, the most intense bands in the L_b (B_{3u}) naphthalene absorption are short axis polarized B_{2u} (i.e. the same symmetry as L_a). Herzberg[17] suggests that this arises from transition to a B_{3u} (L_b) electronic state combined with a vibrational wave function with symmetry B_{1g} to give an overall symmetry B_{2u}. Thus, the IEET process begins by population of the covalent L_b state of naphthalene where the initial nuclear motion is a nontotally symmetric B_{1g} vibration.

Anthracene emission, after IEET, occurs from the lowest energy anthracene L_a hole-pair state. In the A*x*N species, the anthracene L_a zwitterionic state must be entered either (a) directly, after crossing from the initially populated L_b state of naphthalene, or (b) indirectly, after crossing from the L_b state

(8) Speiser, S. *Pure Appl. Chem.* **1992**, *64*, 1481−1487.
(9) Bigman, J.; Karni, Y.; Speiser, S. *Chem. Phys.* **1993**, *177*, 601−617.
(10) Rosenblum, G.; Karni, Y.; Speiser, S. *Isr. J. Chem.* **1997**, *37*, 445−453.
(11) Chattoraj, M.; Bal, B.; Closs, G. L.; Levy, D. H. *J. Phys. Chem.* **1992**, *95*, 9666.
(12) Vreven, T.; Bernardi, F.; Garavelli, M.; Olivucci, M.; Robb, M. A.; Schlegel, H. B. *J. Am. Chem. Soc.* **1997**, *119*, 12687.
(13) Smith, B. R.; Bearpark, M. J.; Robb, M. A.; Olivucci, M.; Bernardi, F. *Chem. Phys. Lett.* **1995**, *242*, 27.
(14) Bearpark, M. J.; Bernardi, F.; Olivucci, M.; Robb, M. A.; Smith, B. R. *J. Am. Chem. Soc.* **1996**, *118*, 5254.
(15) Clifford, S.; Bearpark, M. J.; Bernardi, F.; Olivucci, M.; Robb, M. A.; Smith, B. R. *J. Am. Chem. Soc.* **1996**, *118*, 7353.
(16) Bearpark, M. J.; Bernardi, F.; Clifford, S.; Olivucci, M.; Robb, M. A.; Vreven T. *J. Am. Chem. Soc.* **1996**, *118*, 169.
(17) Herzberg, G. *Electronic spectra and electronic structure of polyatomic molecules*; Van Nostrand: Princeton, NJ, 1950; Vol. 3.

of naphthalene to the L_b state of anthracene along the reaction coordinate Q. We shall give evidence that path b is the preferred mechanism since the anthracene L_a hole-pair state lies lower in energy along the whole reaction path.

In this article, we present a theoretical study of both **A1N** and **A3N** molecules using a hybrid molecular mechanics with valence bond (MMVB) method.[18,19] Nonadiabatic "on the fly" trajectories[20] have been used to study the details of the mechanism of energy transfer. MMVB uses a space of neutral valence bond determinants and has been parametrized against CAS-SCF. The VB part contains exchange parameters that are of the same type as in Heitler−London VB theory. As a consequence, the implicit orbital basis is nonorthogonal and the charge transfer (or ionic) terms are included in the parametrization. However, the wave function does not include true zwitterionic terms so the hole-pair (L_a) states of anthracene and naphthalene cannot be represented. Thus we cannot study the crossing of the L_a and L_b states. Accordingly, we assume (mechanism b just suggested) that the final stage of the IEET process occurs via crossing to the anthracene L_a zwitterionic state from the L_b state of anthracene along the reaction coordinate Q. This hypothesis has been tested by computing (using TD-DFT[21−23] in a 6-31G* basis) the energy of the L_a and L_b states of anthracene, contained in **A3N**, along our reaction coordinate and verifying that the hole-pair (L_a) state of anthracene lies lower in energy than the L_b states everywhere.

As we shall discuss subsequently, we have run only one trajectory starting from the FC geometry itself with no initial momenta in any of the normal modes. Thus the trajectory is the simplest possible generalization of a minimum energy path where the geometry relaxes under the force field of the excited state. If the "local" D_{2h} symmetry were retained for the anthracene and naphthalene chromophores, the trajectory would not traverse geometries corresponding to nontotally symmetric vibrations at all. Of course, experimentally, as suggested by Herzberg,[17] the nontotally symmetric B_{1g} vibration is populated upon excitation to the naphthalene L_b state. Thus, a more realistic simulation might have been run with initial momentum in the nontotally symmetric B_{1g} normal mode. In this case, the system could behave in two different ways: (a) either the system would fall off a "ridge", if the space of non-totally symmetric vibrations had components that were negatively curved (imaginary frequencies) or (b) if the space is positively curved, one would simply see a population of nontotally symmetric oscillations superimposed on totally symmetric motions. However, no symmetry restrictions are imposed on our trajectories and the molecular systems have no symmetry overall. Thus the trajectories are free to explore geometries that break local D_{2h} symmetry (i.e. to fall off a "ridge" if it existed). However, in our simulation local nontotally symmetric vibrations of the naphthalene or anthracene are not stimulated. This suggests the space of (local) nontotally symmetric geometries is positively curved. Thus our computed trajectory, which is observed to be confined to the space of totally symmetric geometries, is a reasonable representative of the ensemble of trajectories that one might run following excitation from the FC region.

The triplet states of naphthalene and anthracene lie below the singlet states. These triplet states can combine in A*x*N species to produce a covalent state of singlet spin multiplicity. (Such a state is seen even in butadiene where the covalent dark state can be interpreted in terms of two coupled ethylene triplets.) This covalent state (denoted by **N*-A***) can be correctly treated in our MMVB model. Our computations suggest that this third state, a "dark" state since it cannot be seen in absorption or emission, is involved in IEET because it becomes the lowest energy covalent state at a local minimum along the coordinate Q and thus must control the dynamics in the intermediate region.

Since we are considering only covalent states we adopt the following notation convention througout the paper. We shall use S_1, S_2, and S_3 to denote the relative energetic ordering of the covalent states (even though the anthracene L_a state lies below the lowest energy covalent state in our computations). We will use **N*-A**, **N*-A***, and **N-A*** to indicate the diabatic state (i.e. the electronic configuration and spin coupling) irrespective of the energy ordering.

The qualitative picture of IEET that emerges from our computations is summarized in Scheme 1, paths b to d. In Scheme 1b we show the picture corresponding to Scheme 1a in the space of two coordinates, denoted **N*-A** and **N-A***, corresponding to geometrical distortion of the naphthalene and anthracene chromophores along the transannular bonds. In this picture Q still connects the **N*-A** and **N-A*** potential minima. However, there is the third state (not shown in Scheme 1b) involved in IEET **N*-A***, the state where both chromophores are triplet excited. It must control the dynamics in the intermediate region as illustrated in Scheme 1, paths c and d. In other words, if the potential curves shown in Scheme 1a are extended into the middle region, the two curves cross and another state, **N*-A***, intervenes and becomes the lowest in energy along a coordinate perpendicular to Q as shown in paths c and d in Scheme 1.

As we shall discuss in detail, the initial excitation of the naphthalene chromophore at the ground-state equilibrium geometry (the Franck−Condon point denoted FC in Scheme 1b) populates a higher excited state (S_3 in Scheme 1d). Decay along the **N*-A** coordinate leads to the **N*-A** equilibrium geometry, but occurs only after passing through two conical intersections shown schematically in Scheme 1d (and denoted CI in Scheme 1b where the **N*-A*** state is omitted for simplicity). Thus the relaxation process after **N*-A** excitation involves a photochemical nonadiabatic process involving three electronic states.

Thus the conical intersections that have been involved in radiationless decay processes for photochemical mechanisms[24−26] and which are known to provide a common fast decay channel from the lowest excited states (for review see ref 27) seem to be involved in IEET as well. However, while the first step of the reaction is photochemical, we will show that the IEET process occurs on the lowest energy covalent potential surface (which changes diabatically from **N*-A** to **N*-A*** and **N-A***), and corresponds essentially to a intramolecular vibrational

(18) Bernardi, F.; Olivucci, M.; Robb, M. A. *J. Am. Chem. Soc.* **1992**, *114*, 1606−1616.
(19) Bearpark, M. J.; Bernardi, F.; Olivucci, M.; Robb, M. A. *Chem. Phys. Lett.* **1994**, *217*, 513−519.
(20) Klein, S.; Bearpark, M. J.; Smith, B. R.; Robb, M. A.; Olivucci, M.; Bernardi, F. *Chem. Phys. Lett.*
(21) Gross, E. K. U.; Kohn W. *Adv. Quantum Chem.* **1990**, *21*, 255.
(22) Casida, M. E. *Recent advances in density functionnal methods*; Chong, D. P., Ed.; World Scientific: Singapore, 1995; Vol. 1.
(23) Casida, M. E. *Recent developments and applications of modern density functionnal theory, theoretical and computational chemistry*; Seminario, J. M., Ed.; Elsevier: Amsterdam, 1995; Vol. 4.
(24) Teller, E. *Isr. J. Chem.* **1969**, *7*, 227−235.
(25) Zimmerman, H. E. *J. Am. Chem. Soc.* **1966**, *88*, 1566−1567.
(26) Michl, J. *J. Mol. Photochem.* **1972**, 243−255.
(27) Bernardi, F.; Olivucci, M.; Robb, M. A. *Chem. Soc. Rev.* **1996**, *25*, 321−328.

redistribution (IVR) process (Scheme 1c). This is followed by decay into the anthracene L_a state with emission which we have not studied.

Computational Methods

Full geometry optimizations and dynamics studies for the ground and excited states of both molecules have been carried out using the hybrid quantum mechanical/force field method MMVB (molecular mechanics valence bond) that simulates CASSCF results.[18,19] MMVB is a hybrid method, which uses the MM2 potential[28] to describe an inactive molecular framework and a Valence Bond (VB) (or Heisenberg) Hamiltonian[29−32] for the active electrons. In our studies, the bridge between the two chromophores (1 and 3 methyl groups for **A1N** and **A3N**, respectively) and the σ molecular frame constitute the inert molecular framework, while the π systems of naphthyl and anthryl groups are represented by the Valence Bond Hamiltonian. A set of molecular VB parameters is presently available for sp^2/sp^3 carbon atoms and this algorithm has been recently "benchmarked" against CASSCF for styrene and indene photophysics.[33]

Studies of the short time scale excited-state relaxation following the specific vertical excitation of the naphthyl moiety have been carried out, for both systems, by performing nonadiabatic "on the fly" dynamic calculations at the MMVB level.[20] In such semiclassical dynamics, the electronic wave function is propagated using time-dependent quantum mechanics in synchronization with nuclear propagation using classical mechanics. Thus mixed state propagation[34,35] has been used to describe the nonadiabatic transition. In this method, the nuclear dynamics are controlled by the Ehrenfest force and the trajectory "feels" the potential surfaces and the nonadiabatic couplings all the time. This approach allows one to describe trajectories where the molecular system re-crosses the region of strong coupling many times. The Franck−Condon region has been chosen as the starting point of the trajectories and no initial kinetic energy has been added. No symmetry constraints are imposed and the system is free to explore geometries where the local D_{2h} symmetry is not retained. As mentioned in the Introduction, the anthracene and naphthalene subspecies undergo totally symmetric skeletal vibrations so one may conclude that the space of nontotally symmetric vibrations is positively curved.

The π systems of naphthyl and anthryl groups yield a rather large VB expansion consisting of about 3×10^6 configurations for the 24 active electrons. Thus computing resources for the geometry optimizations and dynamics are dominated by the time required for the eigenvalue determination for 3×10^6 configurations. Accordingly, the dynamics simulations must be limited to very small regions of phase space because of computing time requirements. Given this constraint, we would not pretend that the dynamics information itself can be directly related to experiment. Rather, the dynamics computations are being used to determine the general topology of the potential surface and to decide which regions of the potential surface may control IEET.

Finally, we wish to interpret the nature of the electronic states involved in the IEET process. Clearly it is impossible to inspect the electronic configurations in a vector with 3×10^6 configurations. Thus for qualitative analysis we use the "exchange" density matrix element P_{ij} where i and j are carbon atom sites (see for example ref 18). The physical interpretation of the "exchange" density matrix is related to the spin coupling between electrons i and j. The "ideal" P_{ij} is $+1$ for pairs of singlet coupled electrons, $-1/2$ for uncoupled pairs, and -1 for triplet spins pairing.

Table 1. A3N TD-DFT vs MMVB Vertical Excitation Energies Computed at the Starting Geometry (FC) and at the N-A*(L_b) Geometry

	A3N FC geometry		A3N N-A*(L_b) geometry	
	TD-DFT	MMVB	TD-DFT	MMVB
N-A*(L_a)	68 ($f = 0.052$)		60 ($f = 0.045$)	
N-A*(L_b)	77 ($f = 0.005$)[a]	77	76 ($f = 0.013$)[a]	63
N*(T_1)-A*(T_1)	84 ($f = 0.012$)[a]	84	78 ($f = 0.004$)[a]	76
N*(L_b)-A	88 ($f = 0.003$)[a]	88	82 ($f = 0.002$)[a]	88
N*(L_a)-A	98 ($f = 0.017$)		88 ($f = 0.024$)	

[a] Since TD-DFT gives only the projection of the wave function onto the space of single excitations, the assignment of the covalent (L_b and N*-A*) TD-DFT states is ambiguous. The L_a states are just HOMO-LUMO excitations.

As discussed in the Introduction, since MMVB cannot treat the L_a hole-pair states, we must make the assumption that the covalent state (i.e. L_b states plus the **N*-A*** state formed by the combination of two triplets) lies in a band bordered by the L_a states along the reaction path of our trajectories. Accordingly, we have carried out TD-DFT computations in a 6-31G* basis at several points along our computed reaction path and the results for two points are given in Table 1.

The comparison of TD-DFT results with MMVB is not straightforward. First, the orbitals of the two chromophores may be mixed in the ground state DFT computation. Second, the TD-DFT wave function contains only the projections on the space of singly excited states. Thus for a state that is dominated by a double excitation, the wave function shows only a pair of single excitations. Thus, while the nature of the L_a states can be determined unambiguously from the orbital excitation pattern (HOMO-LUMO) and the oscillator strengths (f in Table 1), only the oscillator strengths can be used to identify the L_b and the **N*-A*** state. The MMVB wave functions can be analyzed using the "exchange" density matrix just discussed so the assignments are unambiguous here.

The **N-A***(L_a) anthracene state (see the first row in Table 1) can be identified unambiguously from the TD-DFT computations and lies some 10−15 kcal mol^{-1} lower than the covalent manifold of states at all points along the reaction path to be discussed in more detail in the next section. This state is always the simple HOMO-LUMO excitation with a significant computed oscillator strength. At the two points presented in Table 1, the anthracene and naphthalene orbitals are not strongly mixed so that the naphthalene L_a state can also be unambiguously assigned and results from a pure HOMO-LUMO excitation of the naphthalene species. The covalent L_b states and the **N*-A*** state can be identified in the TD-DFT computations only from the oscillator strengths and from the occurrence of the homo/lumo+1 and homo−1/lumo single excitation patterns. It is not possible to assign the TD-DFT results further than this. However, these results do give a strong indication that the assumption that the reaction path can be traced out in the manifold of covalent states and that the **N-A***(L_a) anthracene state lies lower in energy everywhere along the reaction coordinate and the **N*-A**(L_a) lies higher is justified.

In Table 2, we give experimental 0−0 excitation energies,[36−48] with the vertical TD-DFT and MMVB results for the isolated chromophores. These data give a general indication of the accuracy of our MMVB results. While TD-DFT gives the L_a state of naphthalene slightly more

(28) Allinger, N. L. *Adv. Phys. Org. Chem.* **1976**, *13*, 1.
(29) Anderson, P. W. *Phys. Rev.* **1959**, *115*, 2.
(30) Said, M.; Maynau, D.; Malrieu, J.-P.; Bach, M.-A. G. *J. Am. Chem. Soc.* **1984**, *106*, 571.
(31) Said, M.; Maynau, D.; Malrieu, J.-P. *J. Am. Chem. Soc.* **1984**, *106*, 580.
(32) Durand, P.; Malrieu, J.-P. *Adv. Chem. Phys.* **1987**, *67*, 321.
(33) Bearpark, M. J.; Bernardi, F.; Olivucci, M.; Robb, M. A. *J. Phys. Chem. A* **1997**, *101*, 8395−8401.
(34) Amarouche, M.; Gadea, F. X.; Durup, J. *Chem. Phys.* **1989**, *91*, 145.
(35) Domcke, W.; Stock, G. *Adv. Chem. Phys.* **1997**, *100*, 1.
(36) Ferguson, J.; Mau, A. W. H. *Mol. Phys.* **1974**, *28*, 469.
(37) Lambert, W. R.; Felker, P. M.; Syage, J. A.; Zewail, A. H. *J. Chem. Phys.* **1984**, *81*, 2195.
(38) Lambert, W. R.; Felker, P. M.; Zewail, A. H. *J. Chem. Phys.* **1984**, *81*, 2209.
(39) Peng, L. W.; Keelan, B. W.; Semmes, D. H.; Zewail, A. H. *J. Phys. Chem.* **1988**, *92*, 5540.
(40) Wolf, J.; Hohlneicher, G. *Chem. Phys.* **1994**, *181*, 185.
(41) Swiderek, P.; Michaud, M.; Hohlneicher, G.; Sanche, L. *Chem. Phys. Lett.* **1990**, *175*, 667.
(42) Allan, M. *J. Electron Spectrosc.* **1989**, *48*, 219.
(43) *UV atlas of organic compounds*; Butterworths/Verlag Chemie: London/Weinheim, 1966−1971.
(44) George, G. A.; Morris, J. *J. Mol. Spectrosc.* **1968**, *26*, 67.
(45) Huebner, R. H.; Meilczarek, J. R.; Kuyait, C. E. *Chem. Phys. Lett.* **1972**, *16*, 464.

Table 2. TD-DFT vs MMVB Vertical Excitation Energies (kcal mol^{-1}) for Isolated Chromophres

	anthracene			naphthalene		
	T_1	L_a	L_b	T_1	L_b	L_a
exp 0−0	42−43[a]	76−79[b,c]	80−87[c]	60−69[d,e]	91−95[f−i]	100−110[d,f,g,i]
TD-DFT[k]	43	77 ($f = 0.057$)	88 ($f = 0.002$)	64	102 ($f = 0.000$)	100 ($f = 0.053$)
MMVB[k]	38		77	46	88	

[a] Reference 48. [b] Reference 44−46. [c] Reference 47. [d] Reference 42. [e] Reference 43. [f] Reference 38. [g] Reference 39. [h] Reference 40. [i] Reference 36−37. [j] Reference 41. [k] Computations carried out using MMVB optimized S_0 geometries.

stable than the L_b state, the agreement between TD-DFT and experimental 0−0 excitation energies is in general good, which means that the TD-DFT (Table 1) can serve as a useful guide against which to calibrate the A*x*N results. The MMVB results for the covalent states consistently underestimate experimental values although the difference E(**N***(L_b)) − E(**A***(L_b)) is well reproduced. The differences between TD-DFT and MMVB results are significantly smaller for A*x*N as shown in Table 1. This is typical of MMVB (see benchmark results in ref 33) and arises partly due to a cancellation of errors in larger systems (i.e. errors for isolated anthracene are smaller than for isolated naphthalene). Notice, that while the sum of the two triplet MMVB energies for the isolated chromophores underestimates the experimental or TD-DFT values (largely as a result of the naphthalene data), this type of error is not seen in Table 1 (for the **A3N** FC geometry).

Results and Discussion

The Region of FC Geometry, the N*-A and N-A* Minima, and the Conical Intersection. In this section we shall document the potential energy surfaces for both systems in the region of the ground-state equilibrium geometry, the region of the **N*-A** and **N-A*** minima on the lowest energy covalent state, and the **N*-A/N-A*** conical intersection (see Scheme 1b). This information, in turn, suggests the choice of the initial geometries and electronic states for the dynamics computations that will be discussed in the next subsection.

We begin with a discussion of the ground-state equilibrium geometry of **A3N** and **A1N**. Our MMVB optimizations for **A3N** yield two different minima: an "open" type conformation (noted **A3No)** shown in Figure 2a and an anthracene−naphthalene face-to-face "sandwich" type conformation (noted **A3Ns**) shown in Figure 2b. The anthracene and naphthalene moieties are planar in both structures. The energy difference between these two structures is 0.4 kcal mol^{-1}, which would imply a 40% population of **A3Ns** at the experimental temperature.[3] The average interplane distance in **A3Ns** is about 3.6 Å consistent with the structure calculated with MM2 and AMBER molecular force field methods.[3] In contrast, the **A1N** ground-state minimum adopts a "T shape" conformation where the angle between the planes of the two chromophores is close to 80° (see Figure 2c). Thus the interchromophore interaction should be negligible in **A1N** and **A3No**. Accordingly, to simulate the effects of interchromophore interaction on the relaxation process, the **A1N** and **A3Ns** structures have been used for the dynamics calculations.

B3LYP/3-21G[49−55] ground-state geometry optimizations have also been carried out using the Gaussian package.[56] For **A1N**, the angle between the two chromophores planes is close to 90° with the B3LYP method in agreement with MMVB and for **A3No** conformation, the B3LYP geometry is almost identical with that of MMVB. In contrast, starting from the MMVB optimized geometry for the **A3Ns** conformation, the B3LYP method converges to a different conformation, where the naphthalene plane is tilted by 30° some ca. 6 kcal mol^{-1} above **A3No**. This is not surprising since DFT cannot represent dispersive forces. Force field methods have a parametrization of the van der Waals interaction and do not give rise to such problems. Zehnacker et al.[57] have encountered similar problems

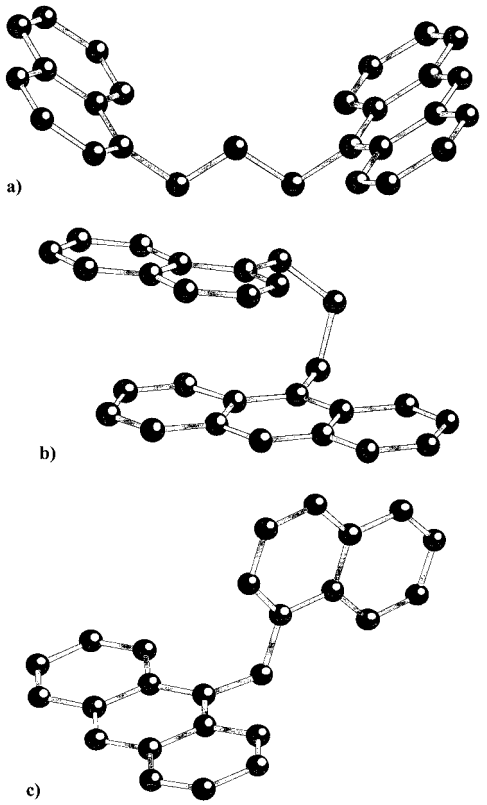

Figure 2. Optimized ground-state geometries: (a) MMVB **A3N** "open" type conformation, (b) MMVB **A3N** "sandwich" type conformation, and (c) MMVB **A1N** "T" type conformation.

(46) Mikani, N.; Ito, M. *Chem. Phys. Lett.* **1975**, *31*, 472.
(47) Dick, B.; Hohlneicher, G. *Chem. Phys. Lett.* **1981**, *84*, 471.
(48) McConey, J. W.; Trajmar, S.; Man, K. F.; Ratliff, J. M. *J. Phys. B* **1992**, *25*, 2197.
(49) Becke, A. D. *J. Chem. Phys.* **1993**, *98*, 5648.
(50) Lee, C.; Yang, W.; Parr, R. G. *Phys. Rev.* **1988**, *B37*, 785.
(51) Binkley, J. S.; Pople, J. A.; Hehre, W. J. *J. Am. Chem. Soc.* **1980**, *102*, 939.
(52) Gordon, M. S.; Binkley, J. S.; Pople, J. A.; Pietro, W. J.; Hehre, W. J. *J. Am. Chem. Soc.* **1982**, *104*, 2797.
(53) Pietro, W. J.; Francl, M. M.; Hehre, W. J.; Defrees, D. J.; Pople, J. A.; Binkley, J. S. *J. Am. Chem. Soc.* **1982**, *104*, 5039.
(54) Dobbs, K. D.; Hehre, W. J. *J. Comput. Chem.* **1986**, *7*, 359.
(55) Dobbs, K. D.; Hehre, W. J. *J. Comput. Chem.* **1987**, *8*, 861. Dobbs, K. D.; Hehre, W. J. *J. Comput. Chem.* **1987**, *8*, 880.
(56) Frisch, M. J.; Trucks, G. W.; Schlegel, H. B.; Scuseria, G. E.; Robb, M. A.; Cheeseman, J. R.; Zakrzewski, V. G.; Montgomery, J. A.; Stratmann, R. E., Jr.; Burant, J. C.; Dapprich, S.; Millam, J. M.; Daniels, A. D.; Kudin, K. N.; Strain, M. C.; Farkas, O.; Tomasi, J.; Barone, V.; Cossi, M.; Cammi, R.; Mennucci, B.; Pomelli, C.; Adamo, C.; Clifford, S.; Ochterski, J.; Petersson, G. A.; Ayala, P. Y.; Cui, Q.; Morokuma, K.; Malick, D. K.; Rabuck, A. D.; Raghavachari, K.; Foresman, J. B.; Ortiz, J. V.; Baboul, A. G.; Cioslowski, J.; Stefanov, B. B.; Liu, G.; Liashenko, A.; Piskorz, P.; Komaromi, I.; Gomperts, R.; Martin, R. L.; Fox, D. J.; Keith, T.; Al-Laham, M. A.; Peng, C. Y.; Nanayakkara, A.; Gonzalez, C.; Challacombe, M.; Gill, P. M. W.; Johnson, B.; Chen, W.; Wong, M. W.; Andres, J. L.; Gonzalez, C.; Head-Gordon, M.; Replogle, E. S.; Pople, J. A. Gaussian 99, Development Version (Revision A.9); Gaussian, Inc.: Pittsburgh, PA, 1998.

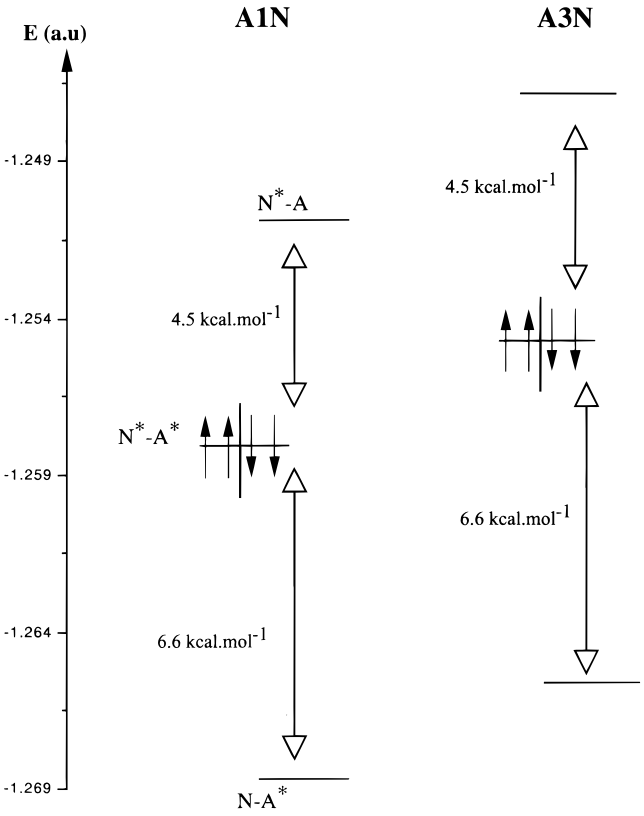

Figure 3. Energy level diagram showing the **N-A***, **N*-A***, and **N*-A** excited states for **A1N** and **A3N** at the Franck−Condon region.

with the AM1 method. The **A3Ns** conformation has been used as the FC geometry in our simulations.

We now turn to a discussion of the excited-state manifold at the Franck−Condon geometry for **A1N** and **A3N**. The results are summarized in Figure 3. In addition to the **N*-A** singlet state (excitation of the naphthyl moiety) and **N-A*** (excitation of the anthracene) singlet state, which are characterized as S_3 and S_1, respectively, one obtains a state S_2, which we denote as **N*-A***. The S_2 **N*-A*** excited state corresponds to two triplet excited **N*** and **A*** subsystems coupled overall to a singlet (see the graphical representation in Figure 3). The absorption to or emission from **N*-A*** is forbidden and this state may not be detected easily in experiments.

The differences (Figure 4) of P_{ij} between S_0 and S_n confirm the electronic assignment just discussed. If one does not consider the interchromophoric terms, the exchange density matrix elements P_{ij} of **A1N** are almost identical with that of **A3N**. Thus $\Delta P_{ij}(S_0-S_1)$ where S_1 is **N-A*** shows large changes in the coupling involving the anthracene and no change for naphthalene as expected. For $\Delta P_{ij}(S_0-S_2)$ where S_2 is **N*-A*** there are large changes in the coupling involving both the anthracene and naphthalene. Finally, for $\Delta P_{ij}(S_0-S_3)$ where S_3 is **N*-A**, only large changes in the coupling of the naphthalene are observed. In all cases, the most important P_{ij} modifications involve the intrachromophore transannular bonds. In general, the P_{ij} corresponding to interchromophoric spin coupling all have the theoretical value of -0.5 corresponding to uncoupled pairs. The exceptions are the interchromophoric spin couplings for **N*-A*** in **A1N** and for all the excited states in **A3Ns**. The computed P_{ij} here are less negative than the theoretical value of -0.5, indicating weak interchromophoric singlet coupling.

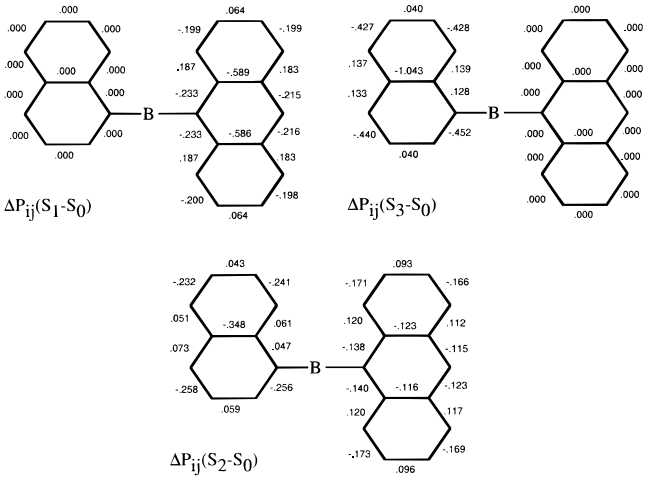

Figure 4. "Exchange" density matrix differences $[\Delta P_{ij}(S_m - S_n) = P_{ij}(S_m) - P_{ij}(S_n)]$ between the ground state (S_0) and the three excited states (S_1, S_2, S_3) at the Franck−Condon region. Only the intrachromophoric terms are shown. The numbers are the same for **A1N** and **A3N** (B = CH_2 or $(CH_2)_3$).

To conclude this section, we discuss the excited-state equilibrium geometries of **N*-A** and **N-A*** as well as the **N*-A**/**N-A*** conical intersection. Although at the Franck−Condon geometry the **N*-A** state is S_3, the minimum of the **N*-A** electronic state occurs on S_1. We refer to this state as **S_1(N*-A)**. Thus the surface (ignoring the **N*-A*** state) has the form shown in Scheme 1b. The **N-A*** state, which is S_1 at the Franck−Condon geometry, is a distinct minimum on S_1, which we denote as **S_1(N-A*)**. In the optimized geometries for S_1-(**N*-A**) and S_1(**N-A***), the interchromophoric geometry parameters are identical (within 0.001 Å and 6° of the ground state). Further, the intrachromophoric parameters are identical to within 0.002 Å for **A1N** and **A3N**. The bond length differences between the ground state and these two excited-state minima are given in Figure 5 (*Z*-matrix corresponding to the equilibrium geometries is given in the Supporting Information). One can see that the S_1(**N-A***) minimum has a relaxed (S_1) excited-state anthracene moiety and a ground-state naphthalene moiety. The second minimum S_1(**N*-A**) has a relaxed excited state naphthalene moiety and a ground-state anthracene moiety and is connected diabatically to the S_3(**N*-A**) state at Franck−Condon geometry. The S_1(**N-A***) minimum is the most stable structure and the energy difference between these two minima is about 11 kcal mol^{-1}. Finally, an **N*-A**/ **N-A*** conical intersection (i.e. ignoring the **N*-A***) state (**CI(S_1/S_2)**) has also been determined. Its geometry is very close to that of the S_1(**N*-A**) minimum (see Figure 5) and the conical intersection is located about 1 kcal·mol^{-1} above this minimum. In this region, the **N*-A*** surface is also almost degenerate with **N*-A** and **N-A***. Thus further optimization of surface crossings is impossible and only dynamics can be used to study this region in more detail.

In summary, an analysis of the **A1N** and **A3N** excited-state manifold via geometry optimization suggests that the potential energy surface has the form shown in Scheme 1b if the **N*-A*** surface is ignored. The S_1(**N*-A**) and S_1(**N-A***) structures corresponding to distinct minima on S_1 and S_1(**N*-A**) correlate diabatically with S_3 in the Franck−Condon region. The **N*-A*** surface lies between **N*-A** and **N-A*** at the Franck−Condon geometry (Figure 3 and Scheme 1d). Thus the initial dynamics which results following excitation of the **N*-A** state to S_3 must involve nonadiabatic motion on three potential energy surfaces.

(57) Zehnacker, A.; Lahmani, F.; Desvergne J. P.; Bouas-Laurent, H. *Chem. Phys. Lett.* **1998**, *293*, 357.

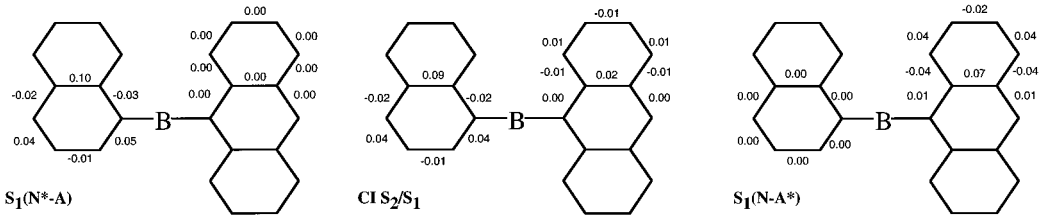

Figure 5. Bond length differences (Å) between the ground state and the two minima on the S_1 potential surface [S_1(**N*-A**) and S_1(**N-A***)] and between the ground state and the S_2/S_1 conical intersection [CI(S_2/S_1)]. The numbers are the same for **A1N** and **A3N** (B = CH_2 or $(CH_2)_3$).

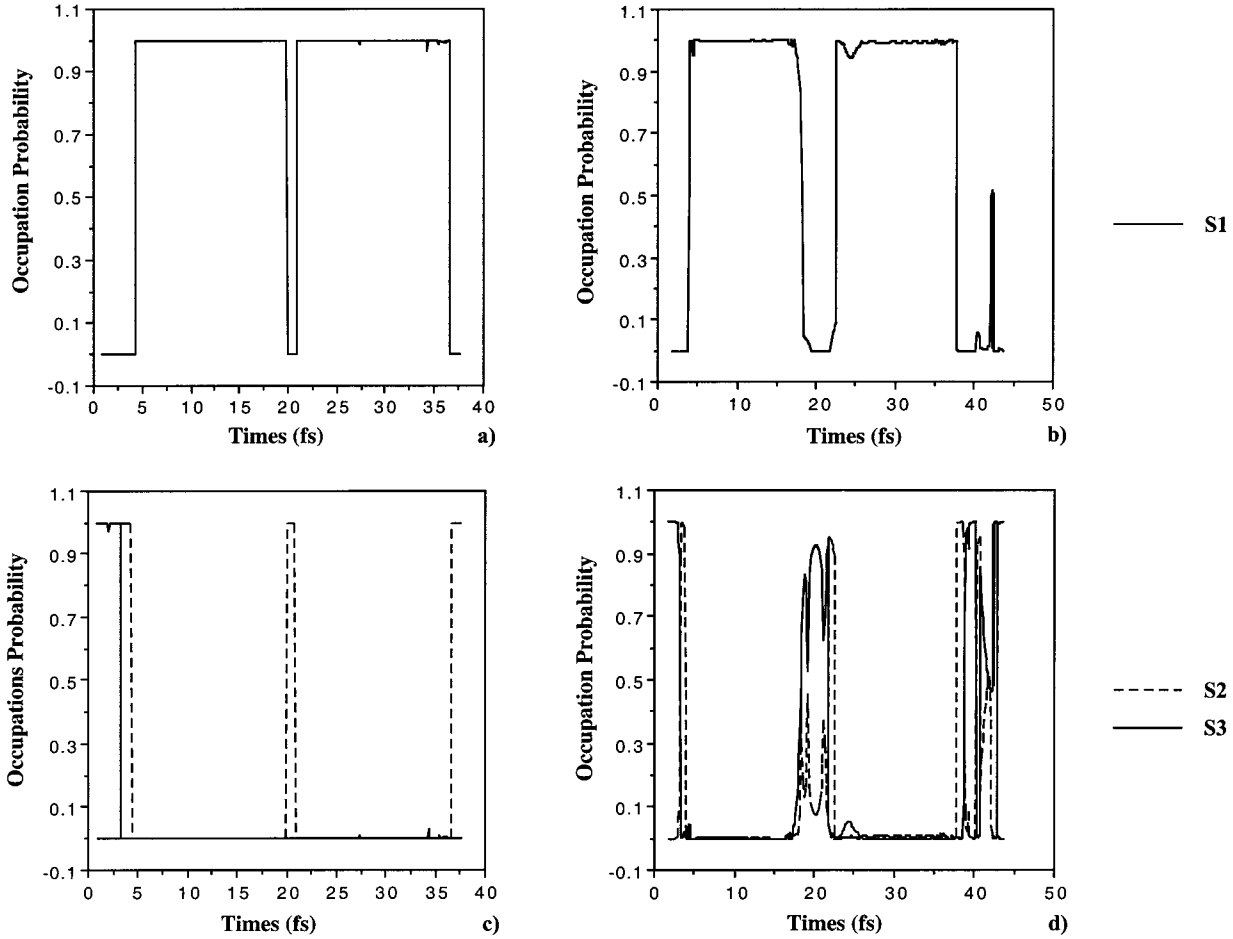

Figure 6. Time dependence of the occupation probabilities for **N-A***, **N*-A***, and **N*-A** dynamics. (a) S_1 occupation for **A1N**; (b) S_1 occupation for **A3N**; (c) S_2 occupation (dotted line) and S_3 (plain line) for **A1N**; and (d) S_2 occupation (dotted line) and S_3 (solid line) for **A3N**.

Dynamics Calculations. In this section we report the results of our dynamics simulations. As stated previously, each time step in the dynamics involves an eigenvalue problem involving 3 million configurations together with the solution of coupled perturbed equations for the gradient of the same dimension. Thus we are limited to exploring a rather limited region of phase space on the basis of trajectories started at the Franck−Condon geometry from the S_3(**N*-A**). Further, we cannot run trajectories for long enough to see the population of intermediate region (see Scheme 1, paths c and d) of the coordinate Q (or the region of the **N-A*** minimum). In the intermediate region of Q (Scheme 1, paths c and d) it is the **N*-A*** surface that is lowest in energy and the overall S_1 surface topology has the form shown in Scheme 1c. To prove that this is the case, and to illustrate the long time decay into the **N-A*** minimum, we have also run trajectories from the Franck−Condon geometry on the **N*-A*** surface. Again, our purpose in the dynamics computations is to determine the topology of the potential surface and to decide which regions of the potential surface may control IEET.

We begin with a discussion of dynamics starting from S_3-(**N*-A**) Franck−Condon geometry to characterize the initial step in the energy transfer process. Thus we discuss dynamics using three singlet excited states (**N-A***, **N*-A***, and **N*-A**). These computations are subject to severe technical limitations. Because we must maintain a very accurate wave function during propagation on three electronic states, a very short time step (0.1 fs) is required and it is possible to run the trajectories only for about 40 fs (each trajectory needs about 20 days of CPU time on a contemporary workstation)

In Figure 6 we show the populations of S_3, S_2, and S_1 for both systems as a function of time. One can see that after a fast nonadiabatic decay from S_3 to S_2 then to S_1, both systems remain about 15 fs on the S_1 potential surface before going back up to the upper surfaces. Notice that the decay from one state to the next is instantaneous (i.e. a pure diabatic surface hop) and that the trajectory involves oscillations that cover three electronic states. The behavior of the transannular bonds of the two chromophores in **A1N** and **A3N** is shown in Figure 7. In both

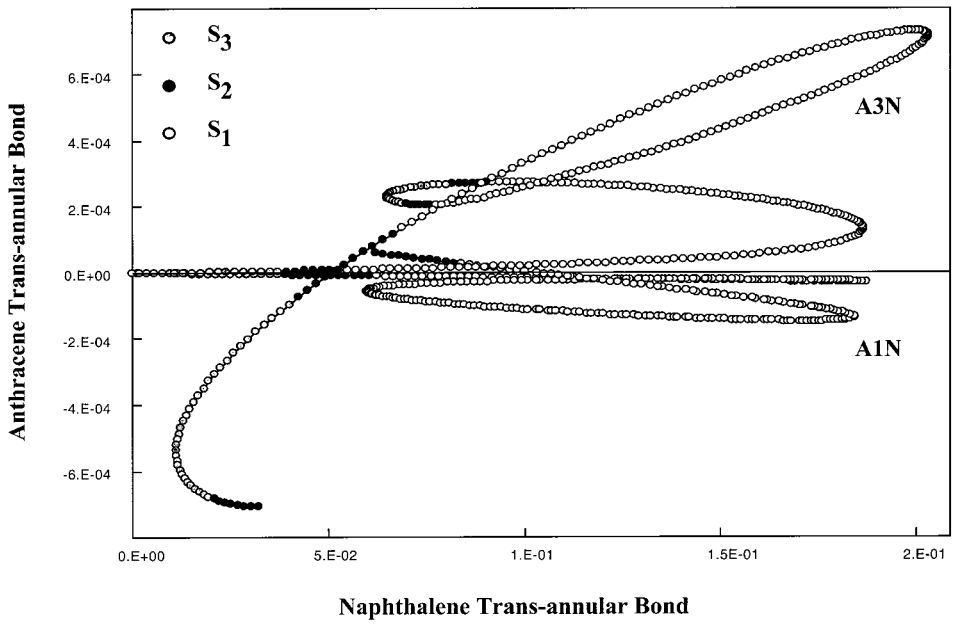

Figure 7. Naphthalene (*x*-axis) vs anthracene (*y*-axis) transannular bonds length differences (Å) relative to the ground-state geometry. The (0,0) coordinate represents the starting point of the trajectories (FC geometry). The open circles indicate that the system is on the S_1 potential surface, the solid circles on S_2 potential surface, and the gray circles on the S_3 potential surface.

A3N and **A1N**, one sees (*x*-axis) a complete relaxation of the naphthalene chromophore through the **N*-A** minimum coupled with much smaller modifications of the anthracene geometry (*y*-axis). The small modifications of the anthracene geometry are four times larger in **A3N** than in **A1N**. Thus even on this short time scale one can observe the flow of energy into the **N-A*** coordinate at a faster rate for **A3N** compared with **A1N**. The origin of the dynamical behavior lies in the couplings existing between the two chromophores. As we have previously discussed the interchromophoric couplings are larger for **A3N** due to the "sandwich" type conformation. Thus this part of the dynamics is consistent with the simple Dexter exchange model.[7] In fact, although the dynamics involves three electronic states, the transitions between these states are essentially diabatic in nature and they are not coupled nonadiabatically.

Referring to Scheme 1c, the penultimate stage of the energy transfer process involves propagation on the **N*-A*** state. While one observes energy transfer into the **N-A*** coordinate in the previous trajectories, it is impossible to run these long enough to observe the propagation on the **N*-A*** surface. Indeed, it has been experimentally determined that the energy transfer process occurs at least in the nanosecond (or longer) time scale. However, along a trajectory started from the S_2(**N*-A***) state in the Franck−Condon region, the S_3 state remains well separated from S_2 and S_1 and the geometry undergoes a simultaneous relaxation of both the naphthalene and anthracene transannular bonds along a coordinate that is almost at right angles to Q in Scheme 1. During this relaxation, the **N*-A*** state crosses the **N-A*** state. Thus the trajectory evolves on an S_2(**N*-A***)−S_1(**N*-A***) surface, recrossing the **N-A*** state in yet another pure diabatic hop. While trajectories run with these initial conditions cannot be directly related to experiment, they do serve to demonstrate the topology of the potential surfaces in the intermediate region of Q (Scheme 1, paths b to d), and illustrate the mechanism of energy transfer from the **N*-A*** surface to the **N-A*** where emission is detected from the L_a state that is ignored here. For these trajectories a much larger time step was possible (1 fs) without losing accuracy. Accordingly, it was possible to run trajectories for up to 450 fs.

The populations of S_2 and S_1 along the trajectories for **A3N** and **A1N** are shown in Figure 8. During the first 200 fs, both the molecular systems develop rapid nonadiabatic oscillations between S_2 and S_1 potential energy surfaces, remaining for less than 20 fs on each surface. Again the transition between the two surfaces is a pure diabatic hop and one is simply seeing motion on the S_2(**N*-A***)−S_1(**N*-A***) diabatic electronic state. The geometry changes occurring during these oscillations are shown in Figure 9. The nuclear motion is the simultaneous concerted motion of both the naphthalene and anthracene transannular bonds. This is consistent with the exchange couplings shown in Figure 4 [$\Delta P_{ij}(S_2-S_0)$] where both the **N** and **A** transannular bonds are partly uncoupled relative to the ground state and both sets of bonds must therefore relax. We have not been able to optimize an S_2(**N*-A***) or S_1(**N*-A***) minimum because the "minimum" occurs at more or less the same geometry as the S_2/S_1 crossing where both sets of transannular bonds lie part way between single and double bonds. However, it has been possible to estimate the energy of this minimum from the dynamic simulations. The **N*-A*** minimum remains about 2 kcal·mol^{-1} below the S_1(**N*-A**) minimum and about 9 kcal·mol^{-1} above the S_1(**N-A***) minimum (Scheme 1c). Nevertheless, no information concerning the energy barrier between S_1(**N*-A**) and S_1(**N*-A***) or between S_1(**N*-A***) and S_1(**N-A***) can be extracted from our computations.

In the case of **A3N**, after about 200 fs, the forces acting on the system finally induce a sudden decrease of the naphthalene transannular bond while the anthracene transannular bonds dramatically increase (see Figure 9). Thus for **A3N**, after 200 fs, the system has passed through a dynamical bottleneck (which may be a transition state) and reaches the S_1(**N-A***) potential well where it will decay finally to the **N-A***(L_a) state. In contrast, no such transfer has been observed for **A1N**, after 440 fs. As we have mentioned before, the singlet interchromophoric couplings are essentially nonnegligible only for **A3N** and this may be the origin of the relative time scales for **A3N** and **A1N**. Thus for the **N*-A*** to **N-A*** process the qualitative ideas

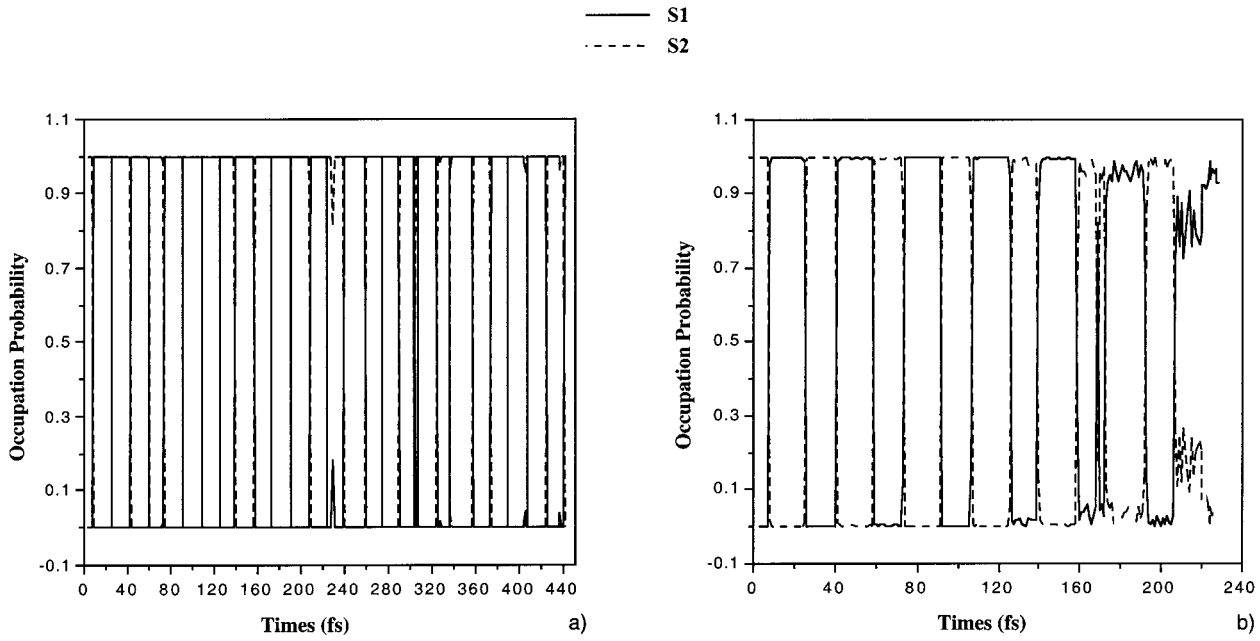

Figure 8. Time dependence of the occupation probabilities for the **N-A*** and **N*-A*** dynamics: S_1 (solid line) and S_2 (dotted line) for **A1N** (a) and **A3N** (b).

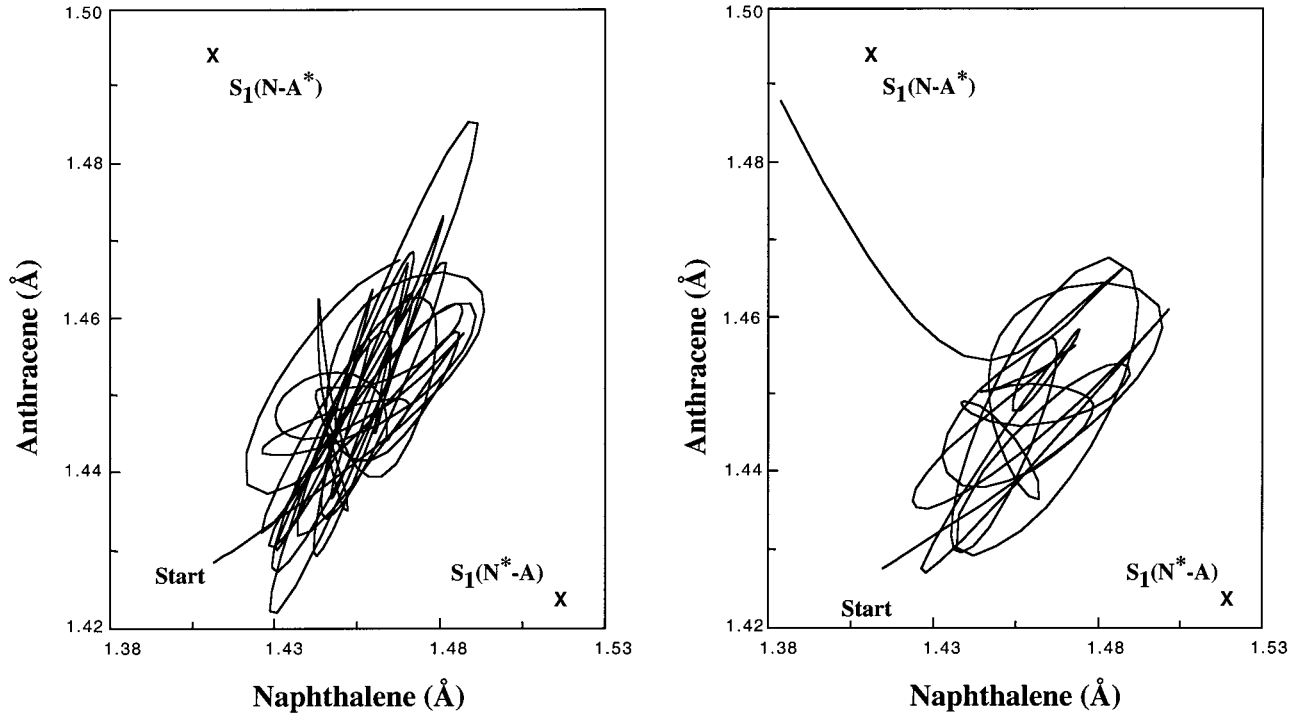

Figure 9. Naphthalene (*x*-axis) vs anthracene (*y*-axis) transannular bond lengths for the **N-A*** and **N*-A*** dynamics: (a) **A1N** and (b) **A3N**.

associated with the short-range exchange interaction model formulated by Dexter[7] may well be a good model.

Conclusions

Semiclassical dynamics simulations at the MMVB level have been used, for the first time, to study the intramolecular electronic energy transfer that occurs in 9-anthryl-1′-naphthylalkane bichromophoric systems. We have shown that a model with two geometric coordinates, the naphthalene transannular bonds (**N*-A** coordinate) and the anthracene transannular bonds (**N-A*** coordinate), and using three covalent excited states, **N***(L_b)-**A**, **N*-A***, and **N-A***(L_b), is needed to accurately describe the mechanistic aspects of IEET. TD-DFT computations show that the three covalent states lie in a band bounded by the hole-pair L_a states of naphthalene and anthracene. Thus the final step of the IEET process involves decay from the anthracene L_b state into the anthracene L_a state followed by emission. This step lies outside of the scope of our computations.

While the dynamics involves nonadiabatic recrossings of several potential surfaces, these recrossings are instantaneous and the system behaves as if motion was occurring on a single diabatic surface so that nonadiabatic couplings do not seem to be important and mixed state propagation is not observed. Our results suggest that a three-step model based on the three **N*-A**, **N*-A***, and **N-A*** "minima" shown in paths c and d in Scheme 1 may be the most appropriate model for IEET. In the

first step, following the photochemical decay into excited vibrational states of the transannular bonds of the naphthalene moiety after specific excitation of the naphthalene coordinate, one has IVR (intramolecular vibrational redistribution) into the anthracene transannular bonds. The rate of this energy transfer seems to be controlled by the interchromophoric exchange interaction as suggested by Dexter (see Figure 7). In the second step, one has dynamics on the **N*-A*** surface followed by the third stage which involves evolution to the **N-A*** minimum. Again the transition from the **N*-A*** surface to **N-A*** minimum appears to be controlled by the interchromophoric exchange interaction and occurs on the S_1 potential surface. The involvement of the **N*-A*** surface has not been considered before in discussions of IEET.

Of course, our study cannot determine which step of the IEET process (Scheme 1c) is rate determining since we cannot run dynamics from the S_3(**N*-A**) surface for a long time. But our studies do indicate that S_1(**N*-A**) IVR into the anthracene transannular bonds is faster for **A3N** where there are weak interchromophoric exchange interactions. Similarly, decay to the **N-A*** minimum from the **N*-A*** surface occurs on a shorter time scale for **A3N**.

The conventional view of IEET is summarized in Scheme 1a. Conventional photochemistry would describe the energy transfer as a direct nonadiabatic process from S_3(**N*-A**) to S_1(**N-A***). Our results indicate that the latter view is not correct and one has a simple "diabatic" decay S_3(**N*-A**) to S_2(**N*-A**) to S_1(**N*-A**) and that IEET occurs on S_1 so that Scheme 1c is a realistic model. Our results do not indicate whether the initial photochemical process (decay from S_3(**N*-A**) to S_1(**N*-A**)) simply prepares a "hot" S_1 reactant involved in the adiabatic energy transfer process or if the photochemical process controls the population of specific vibrational modes which will promote the anthracene relaxation. In view of these observations, modern femtosecond experiments on this system should yield interesting results.

Acknowledgment. F.J. gratefully acknowledges the Marie Curie program from the European Community for a postdoctoral grant (TMR-ERBFMBICT972828). All computations were carried out on an IBM-SP2 funded jointly by IBM-UK and HEFCE (UK). M.A.R. and M.O. are grateful to NATO for a travel grant (CRG 950748). We are also grateful to Josef Michl for helpful discussions.

Supporting Information Available: Atomic numbering scheme used for the geometry description; ground state optimized geometries of **A3No**, **A3Ns**, and **A1N** determined at the MMVB and B3LYP level; S_1(**N-A***), S_1(**N*-A**), and CI(S_1/S_2) optimized geometries of **A3Ns** and **A1N** calculated at the MMVB level; atomic numbering scheme used to describe the spin density matrix; spin density matrix of the ground state, the three first singlets, and the first quintet for **A3No**, **A3Ns**, and **A1N** at the Franck−Condon region (PDF). This material is available free of charge via the Internet at http://pubs.acs.org.

JA992717W